Int. J. Heat Mass Transfer. Vol. 22, pp. 1613–1625.

0017-9310/79/1201-1613 $02.00/0

HEAT-TRANSFER, PRESSURE-DROP AND PERFORMANCE RELATIONSHIPS FOR IN-LINE, STAGGERED, AND CONTINUOUS PLATE HEAT EXCHANGERS

E. M. SPARROW and C. H. LIU†
Department of Mechanical Engineering, University of Minnesota, Minneapolis, Minnesota, U.S.A.

(*Received* 1 *March* 1979 *and in revised form* 17 *April* 1979)

Abstract – Basic heat-transfer and pressure-drop results for laminar airflow through arrays of in-line or staggered plate segments have been determined from numerical solutions of the fluid flow and energy equations. The results depend on only a single dimensionless parameter which encompasses the relevant geometrical and fluid flow quantities. Application of the results was made to compare the performance of the two types of segmented-plate arrays with each other and with the parallel-plate channel. At constant mass flow rate and constant heat-transfer surface area, the heat-transfer effectiveness ε of the segmented arrays is appreciably higher than that of the parallel-plate channel, both in the range of small and intermediate effectiveness values. In addition, for a fixed heat duty corresponding to an intermediate ε value and for a constant mass flow, the heat-transfer area of the segmented arrays is only about a third of that for the parallel-plate channel. Under constant pumping power and constant surface area conditions, the heat transfer for the segmented arrays exceeds that for the parallel-plate channel when the effectiveness of the latter is less than 0.65–0.75. Under most conditions, the staggered array yields better performance than the in-line array, but situations are identified where the reverse is true.

NOMENCLATURE

A_p, surface area of a plate;
c_p, specific heat;
D_h, hydraulic diameter, $4H$;
f, friction factor, equation (19);
H, transverse spacing, Fig. 1;
$\bar{h}_p$, per-plate heat-transfer coefficient, equation (17);
k, thermal conductivity;
L, plate length, Fig. 1;
L_{ex}, heat exchanger length;
$\overline{Nu}_p$, per-plate Nusselt number, equation (18);
$\dot{m}$, mass flow rate;
P, pumping power, equation (21);
Pr, Prandtl number;
p, pressure;
p_i, pressure at inlet;
p_x, pressure at axial station x;
Δp, pressure drop, $p_i - p_x$;
Q, heat-transfer rate for exchanger of length x or L_{ex};
Q_p, heat-transfer rate per plate;
Re, Reynolds number, $\bar{u}(4H)/\nu$;
T_{bx}, bulk temperature at x;
T_i, bulk temperature at inlet;
T_w, plate temperature;
U, V, dimensionless velocities, equation (2);
u, v, velocity components;
$\bar{u}$, mean velocity;
X, Y, dimensionless coordinates, equation (1);
x, y, coordinates, Fig. 1;
ε, heat-transfer effectiveness, equation (14);
θ, dimensionless temperature, equation (6);
μ, viscosity;
ν, kinematic viscosity;
Π, dimensionless pressure, equation (2).

Subscripts

IL, in-line segmented plates;
P, constant pumping power;
S, staggered segmented plates.

Superscript

*, parallel-plate channel.

† Present address: Owens-Corning Fiberglas Company, Granville, Ohio, U.S.A.

INTRODUCTION

IT HAS been recognized for some time that higher convective heat-transfer coefficients can be obtained when a succession of colinear flow-aligned plate segments are employed instead of a single continuous plate. As the fluid passes along such an array of plate segments, a new boundary layer is initiated as each segment is encountered, and it is the thinness of the restarted boundary layers which is responsible for the high coefficients. This characteristic is widely employed in the design of high performance heat exchange devices, as manifested by the use of fin surfaces that are periodically interrupted in the flow direction

(e.g. strip fins). The performance of heat exchangers which incorporate interrupted surfaces has, in the main, been determined from experiments involving actual exchangers or large-scale models (e.g. [1–5]). In [6], the heat-transfer characteristics of an array of offset (i.e. staggered) flow-aligned plate segments was determined via finite-difference solutions of the fluid flow and energy transport equations.

The higher heat-transfer coefficients provided by interrupted surfaces are accompanied by substantial increases in pressure drop, as witnessed by results given in the aforementioned references. Until recently, there was considerable uncertainty as to how to appraise the degree of performance improvement (or degradation) resulting from the conflict between the increase in heat-transfer coefficient and the increase in pressure drop. Methodology for evaluating the benefits of using augmented heat-transfer surfaces (of which interrupted plates are a subset) has been formulated by Bergles and co-workers[7–9]. It was demonstrated that the advantage or disadvantage of using one type of heat-transfer surface relative to another depends upon the goals to be achieved and the constraints of the comparison. The potential goals may include increasing heat transfer or reducing pumping power or reducing the size of the heat exchanger. Possible constraints encompass fixing several among such quantities as the mass flow rate, pressure drop, heat load, heat exchanger size, etc.

From the foregoing, it is evident that there is not a unique appraisal of the merits of an augmented heat-transfer surface; rather, there may be as many different appraisals as there are applications. Therefore, to enable the various types of appraisals to be performed, it is necessary that basic heat-transfer and friction-factor information be available for candidate augmented surfaces.

The present analysis was undertaken to provide such basic information for an array of in-line flow-aligned plate segments and also to employ this information to calculate performance comparisons with related heat-transfer configurations. A schematic diagram of such an array is shown in the upper sketch of Fig. 1. The three-high stack of plates pictured there is intended to portray a much higher stack such that possible end effects at the top and bottom of the stack can be neglected. In addition, the number of streamwise rows is not constrained to that shown in the sketch. The analysis and computations were performed for the case of laminar flow.

The relationship between the in-line array studied here and the offset (i.e. staggered) array of [6] can be clarified with the aid of the figure. If the plates occupying positions AB, CD, EF, etc. were to be moved to positions BC, DE, FG, etc., then the in-line array shown in the upper part of the figure would be transformed to the staggered array shown in the lower part. Under such a transformation, both arrays would have the same amount of heat-transfer surface area but the staggered array would be longer by one row in the streamwise direction.

The initial impetus to undertake the present study came from inquiries (motivated by the publication of [6]) about the relative performance of in-line and staggered strip fin arrays. In the early stages of the work, it was discovered that by proper nondimensionalization, the number of dimensionless parameters could be reduced by one compared with those used in [6], thereby permitting both a more compact and a more general presentation of results than that of [6]. Thus, not only are solutions carried out here for the in-line array, but also the staggered array was solved in terms of the new variables.

Basic heat-transfer and pressure-drop results are presented here for both the in-line and staggered plate arrays as a function of a single parameter which incorporates both the Reynolds number and the ratio of the plate length L to the transverse spacing H. The results encompass both the entrance and fully developed regions. In this regard, it may be noted that a streamwise periodic geometry such as that pictured in Fig. 1 does not admit the same type of fully developed regime as does a conventional duct flow. This matter will be elaborated upon later when the results are presented and discussed.

The basic heat-transfer and pressure-drop results are then employed in various performance comparisons. These comparisons encompass two augmented configurations – the in-line and staggered plate arrays – and the conventional continuous-walled

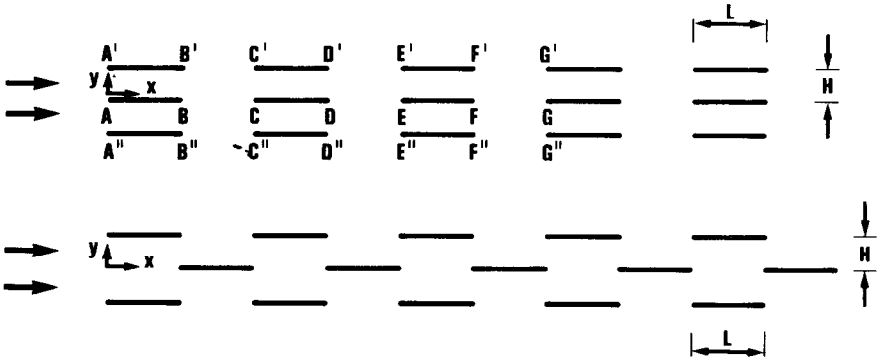

FIG. 1. In-line and staggered plate arrays, upper and lower diagrams, respectively.

parallel-plate channel. Comparisons are first made for the condition of constant mass flow rate, and then the condition of constant pumping power is employed.

The computational scheme employed for the simultaneous fulfillment of the constant pumping power constraint for all three flow configurations is described in some detail. These computations yield the relative magnitudes of the heat-transfer rates for the three configurations at a fixed pumping power. In addition, they reveal the quantitative differences in the Reynolds numbers for the three configurations that are necessary for the attainment of the same pumping power for each. Although it is known that the constant power constraint brings forth such differences in the Reynolds number, the quantitative extent of the differences appears not to have been presented heretofore. The importance of these Reynolds number relationships is underscored by the fact that a heat exchange device is typically implanted in a fluid flow circuit containing other flow resistances. Therefore, a higher (or lower) mass flow through the heat exchanger will have ramifications throughout the entire flow circuit.

ANALYSIS

Formulation of the problem

As was noted earlier, computations will be performed here for both the in-line and staggered arrays in order to enable the results for both configurations to be presented on a common basis. Therefore, the analysis will be framed so that it is applicable to both arrays.

The flow entering the array is at a uniform temperature T_i, and the inlet velocity is uniform and equal to $\bar{u}$. The plates are isothermal (temperature $= T_w$) and are assumed to be sufficiently thin so that thickness effects can be neglected. It is further assumed that laminar flow prevails throughout the length of the array.

If the Kays–London definition [2] is used for the hydraulic diameter, it is readily demonstrated that $D_h = 4H$ for both arrays, and this quantity will, therefore, be used as a reference length. Then, if capital letters are used for dimensionless quantities, the following dimensionless variables may be introduced:

$$X = (x/4H)/Re, \quad Y = y/4H, \tag{1}$$

$$U = u/\bar{u}, \quad V = v(4H)/v, \quad \Pi = p/\rho\bar{u}^2 \tag{2}$$

where Re, the Reynolds number, is given by

$$Re = \bar{u}(4H)/v. \tag{3}$$

With these variables, the mass and momentum conservation equations become

$$\frac{\partial U}{\partial X} + \frac{\partial V}{\partial Y} = 0, \tag{4}$$

$$U\frac{\partial U}{\partial X} + V\frac{\partial U}{\partial Y} = -\frac{d\Pi}{dX} + \frac{\partial^2 U}{\partial Y^2}. \tag{5}$$

Owing to the nondimensionalization, these equations are free of parameters. Then, a dimensionless temperature variable is introduced as

$$\theta = (T - T_i)/(T_w - T_i) \tag{6}$$

and the nondimensional energy equation becomes

$$U\frac{\partial \theta}{\partial X} + V\frac{\partial \theta}{\partial Y} = \frac{1}{Pr}\frac{\partial^2 \theta}{\partial Y^2}. \tag{7}$$

Here, as in equations (4) and (5), geometry and flow parameters have been absorbed into the dimensionless variables, so that, thus far, Pr appears as the only prescribable dimensionless group.

Since this study is directed to tall stacks of plates (i.e. negligible end effects associated with the top and bottom of the stack), attention can be confined to a typical channel defined by $0 \leq y \leq H$ ($0 \leq Y \leq \frac{1}{4}$) and $x > 0$ ($X > 0$). On all solid surfaces bounding such a channel

$$U = V = 0, \quad \theta = 1 \tag{8}$$

whereas on all symmetry boundaries

$$\partial U/\partial Y = V = \partial\theta/\partial Y = 0 \tag{9}$$

and at the inlet

$$U = 1, \quad V = \theta = 0. \tag{10}$$

Thus, the boundary conditions are also free of parameters.

The only dimensionless parameter in the analysis (other than Pr) is the nondimensional plate length

$$(L/4H)/Re \tag{11}$$

which incorporates both the dimensions and the fluid flow rate that characterize the problem.

The governing equations (4), (5) and (7), along with the boundary conditions (8), (9) and (10), were solved by finite differences. The program, which was written specifically for this task, was based on the Patankar–Spalding boundary-layer procedure [10] modified to determine the unknown pressure gradient $d\Pi/dX$ in accordance with the methodology described in the Appendix of [6]. The program was verified by comparison of heat-transfer and pressure-drop results for the staggered array with selected cases of [6]. In addition, results obtained for the continuous-walled parallel-plate channel were compared with those of [6] and [11].

Solutions were carried out for seven values of $(L/4H)/Re$ between 0.0003 and 0.005. This range spans the values of L/H and of the laminar Reynolds number that are relevant to practice. The Prandtl number was fixed at 0.7 (air) for all of the solutions.

Presentation parameters

Attention will now be turned to the output of the numerical solutions and to the variables that have been selected for the presentation of the results. During the execution of the solutions, the bulk temperature T_{bx} at any axial station X was determined by integrating the θ and U distributions as follows:

$$\frac{T_{bx} - T_i}{T_w - T_i} = \theta_b = \frac{\int \theta U \, dY}{\int U \, dY} \tag{12}$$

with the integration extended over the range $0 \leq Y \leq \frac{1}{4}$. Since the rate of heat transfer Q between $X = 0$ and $X = X$ is given by

$$Q = \dot{m} c_p (T_{bx} - T_i) \tag{13}$$

and the heat-transfer rate Q_{max} for an array of infinite streamwise length is

$$Q_{max} = \dot{m} c_p (T_w - T_i) \tag{13a}$$

it follows that $(T_{bx} - T_i)/(T_w - T_i) = Q/Q_{max}$. Moreover, Q/Q_{max} is the heat exchanger effectiveness ε, so that

$$(T_{bx} - T_i)/(T_w - T_i) = \varepsilon. \tag{14}$$

Thus, the dimensionless bulk temperature, when interpreted as the effectiveness, is of direct relevance as a heat exchanger performance parameter. It has, therefore, been selected as one of the quantities for which graphical results will be presented. The distribution of ε along the length of the array will be plotted as a function of the dimensionless streamwise coordinate $(x/4H)/Re$. Since this quantity is a measure of the size (i.e. streamwise length) of the heat exchanger, it can be regarded as the NTU (number of transfer units), although it is different from the conventional definition of NTU. Since heat exchangers are typically made up of an integral number of plates, the ε values at the ends of the successive plates are of primary interest, and these are the values that will be presented here.

If desired, the average heat-transfer coefficient $\bar{h}$ encompassing N rows† between $X = 0$ and $X = NL$ can be readily evaluated from the distribution curves for ε. If

$$\bar{h} = (Q/A)/(\text{LMTD}) \tag{15}$$

and LMTD is the log-mean of $(T_w - T_i)$ and $(T_w - T_{bx})$, then

$$\bar{h}(4H)/k = -RePr \ln(1 - \varepsilon)/(\Omega L/H) \tag{16}$$

where $\Omega = N$ or $\Omega = (N + 1)$, respectively for the staggered and in-line arrays. From the $\bar{h}$ values, the Stanton number St and Colburn j factor can also be determined. These evaluations will not be reported here because of journal space limitations and because ε (which will be reported) is believed to be a more fundamental quantity than the others.

A set of heat-transfer coefficients which will be evaluated and reported are those for the fully developed regime. As noted earlier, periodically varying geometries such as are pictured in Fig. 1 do not yield the same type of fully developed regime as do conventional ducts with continuous walls. Rather, for the multi-plate arrays of Fig. 1, thermal development is attained when the average heat-transfer coefficient per plate is the same for all plates beyond the thermal entrance region. If $\bar{h}_p$ is the average heat-transfer coefficient per plate, then

$$\bar{h}_p = (Q_p/A_p)/(\text{LMTD})_p. \tag{17}$$

The LMTD appearing in equation (17) is based on $(T_w - T_{bx})'$ and $(T_w - T_{bx})''$, where $'$ and $''$ respectively refer to the upstream and downstream ends of a plate. From the definition, it readily follows that

$$\overline{Nu}_p = \bar{h}_p(4H)/k = \frac{RePr}{\Lambda L/H} \ln \frac{1 - \varepsilon'}{1 - \varepsilon''} \tag{18}$$

in which $\Lambda = 1$ for the staggered array and $\Lambda = 2$ for the in-line array. The $\overline{Nu}_p$ results will be tabulated as a function of $(L/4H)/Re$.

With regard to the fluid flow results, the pressure drop is the quantity of most direct practical interest. The pressure information from the solutions was arranged to be printed as $(p_i - p_x)/\frac{1}{2}\rho\bar{u}^2$, where p_i is the inlet pressure and p_x is the pressure at an axial station X. This dimensionless pressure-drop parameter will be plotted as a function of $(x/4H)/Re$ at axial stations corresponding to the ends of the successive plates.

In addition to these pressure distributions, the fully developed friction factor f was evaluated and will be reported. For periodic geometries of the type considered here, the fully developed p vs x distribution is not a straight line as for conventional duct flows. Rather, since the velocity field repeats itself at axial stations x, $(x + 2L)$, ... in the fully developed regime, so do the pressures at x, $(x + 2L)$, $(x + 4L)$, ... lie on a straight line. If the slope of this straight line is dp/dx and if the fully developed friction factor is defined as

$$f = (-dp/dx)D_h/\tfrac{1}{2}\rho\bar{u}^2 \tag{19}$$

then

$$fRe = 2(-d\Pi/dX). \tag{20}$$

Additional computations related to performance comparisons will be described later.

RESULTS AND DISCUSSION

The basic heat-transfer results for the in-line and staggered arrays are presented in Figs. 2 and 3. In both figures, the effectiveness ε, equal to $(T_{bx} - T_i)/(T_w - T_i)$, is plotted as a function of the dimensionless axial coordinate $(x/4H)/Re$ for parametric values of $(L/4H)/Re$. As discussed earlier, the ε values given in the figures correspond to the end points of the successive plates of the array. For the parametric values of $(L/4H)/Re$ appearing in Fig. 2 (i.e. the larger $(L/4H)/Re$), the successive end points are relatively far apart, and the corresponding ε values are plotted as discrete data. The smaller $(L/4H)/Re$ values used to parameterize Fig. 3 give rise to more closely spaced end points, and the ε values have been connected by faired curves.

† For the in-line array, the plates are stacked in the first, third, fifth, etc. rows, so that N is odd.

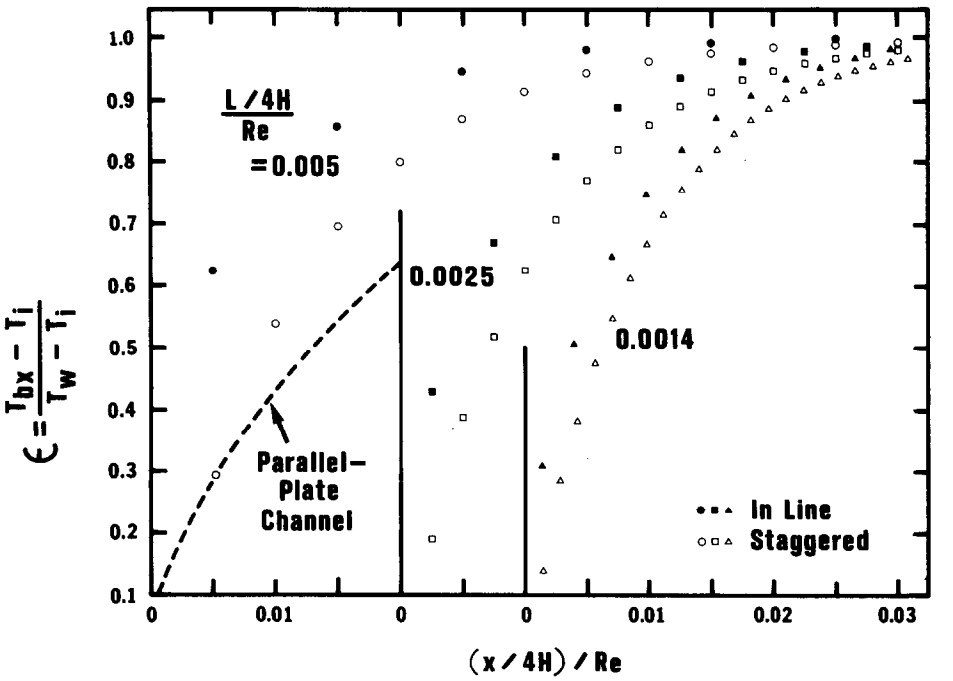

FIG. 2. Heat-transfer effectiveness – range of larger $(L/4H)/Re$.

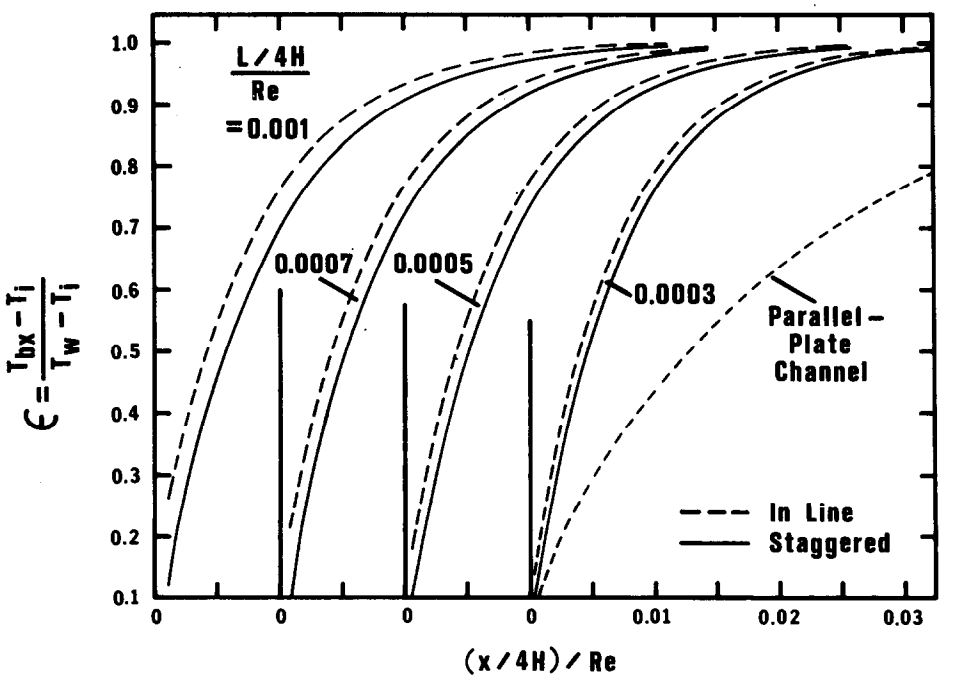

FIG. 3. Heat-transfer effectiveness – range of smaller $(L/4H)/Re$.

The figures have been structured to facilitate comparisons between the in-line and staggered arrays. Each figure is subdivided into several side-by-side panels, and in each panel the ε distributions for the two arrays are plotted for a given value of $(L/4H)/Re$.

In addition to the results for the two types of segmented-plate arrays, Figs. 2 and 3 also show the dimensionless bulk temperature distribution for the conventional parallel-plate channel for $Pr = 0.7$. To ensure a proper comparison between the parallel-plate channel and the segmented arrays, the spacing between the parallel plates of the former should be $2H$. The suitability of this spacing can be verified with the aid of Fig. 1. If, in the upper diagram, the plates occupying positions AB, CD, EF, etc. were to be moved to positions B'C', D'E', F'G', etc., then A'B'C'D'... would form the upper wall of a parallel-plate channel. Similarly, the lower wall A"B"C"D"... would be formed by moving plates up from below. Such a channel, of spacing $2H$, would have the same heat-transfer surface area and hydraulic diameter as both the in-line and staggered arrays. The channel results are, of course, independent of $(L/4H)/Re$ and, to avoid undue clutter, they are included in only the first panel of Fig. 2 and last panel of Fig. 3 (highest and lowest values of $(L/4H)/Re$).

From an inspection of Figs. 2 and 3, it is seen that for all cases, the effectiveness is relatively low for arrays that are short in length (i.e. small $(x/4H)/Re$). As the length of the array increases (i.e. greater number of plates), the effectiveness increases and approaches a limiting value of unity. At a fixed value of $(L/4H)/Re$, examination of any one of the panels in Figs. 2 and 3 shows that the effectiveness of the in-line array exceeds that of the staggered array. The difference in the effectivenesses is most marked at the larger values of $(L/4H)/Re$ (Fig. 2) and diminishes as $(L/4H)/Re$ decreases (Fig. 3). The effectiveness values for the parallel-plate channel lie below those for the segmented-plate arrays, with the deviations being most marked at small $(L/4H)/Re$.

The higher effectiveness values for the in-line array merit some explanation. Part of the difference stems from the fact that at any $(x/4H)/Re$ where effectiveness data are plotted in Figs. 2 and 3 (i.e. at plate end points), the in-line array has more heat-transfer surface than the staggered array. This can easily be verified by examining Fig. 1 (compare, for example, the respective surface areas between $x = 0$ and $x = 5L$ for the two arrays). Even when the area difference is taken into account, the effectiveness of an in-line array continues to exceed that of a corresponding staggered array. The reason for this is that higher local velocities are developed in the more closely spaced passages of the in-line array (for the same mean velocity). As will be demonstrated shortly, the higher velocities have important pressure-drop ramifications.

Careful comparison of the results shown in the successive panels indicates that somewhat higher effectivenesses are attained in the presence of shorter plate segments, that is, for smaller values of $(L/4H)/Re$. Such an examination also reveals that the staggered-array effectivenesses are more sensitive to $(L/4H)/Re$ than are the effectivenesses for the in-line array. This can be easily affirmed by comparing the results for the two arrays with those for the parallel-plate channel, which are plotted in the first and last panels.

The substantial gains in heat-transfer effectiveness that accrue from using segmented plates rather than continuous parallel plates are evident from the figures. It should be noted, however, that for sufficiently large $(x/4H)/Re$, the gains become marginal since ε approaches unity for all of the investigated configurations.

Attention will now be turned to the pressure distributions that are presented in Figs. 4 and 5. In these figures, the dimensionless pressure drop between the inlet at $x = 0$ and axial stations x which correspond to the end points of the successive plate segments is plotted as a function of $(x/4H)/Re$. The structure of Figs. 4 and 5 is patterned after that of Figs. 2 and 3, with separate panels for the various $(L/4H)/Re$ and with either discrete data or faired curves used to represent the results.

From Figs. 4 and 5, it can be seen that except at small $(x/4H)/Re$, the pressures at the successive end points decrease linearly along the length of the array (i.e. $p_i - p_x$ increases). For all of the conditions investigated, the pressure drop for the in-line array is larger than that for the staggered array. Thus, the higher heat-transfer effectiveness of the in-line array is bought at the price of a higher pressure drop. The greatest pressure deviations between the two arrays are at the larger values of $(L/4H)/Re$ (i.e. longer plates), and the smallest differences occur for the shorter plates. Furthermore, there is a general tendency for larger pressure drops to be sustained at smaller $(L/4H)/Re$ (i.e. shorter plates), with this trend being more marked for the staggered array than for the in-line array. These characteristics are identical to those for the effectivenesses that were noted earlier.

It may further be seen that the pressure drops sustained by both of the segmented-plate arrays are substantially larger than that for the parallel-plate channel. This is an expected result and, as will be demonstrated later, it does not necessarily subvert the overall benefit of using an augmented heat-transfer surface.

The heat-transfer and pressure-drop results for the fully developed regime will now be presented. As noted earlier, the per-plate Nusselt number $\overline{Nu}_p$ defined by equations (17) and (18) is a constant in the fully developed regime. In addition, the friction factor f of equations (19) and (20) is also a constant, where the pressure gradient appearing in f corresponds to the pressures at the end points of the successive plates.

The $\overline{Nu}_p$ and fRe values for the two arrays are listed in Table 1 as a function of the dimensionless plate length parameter $(L/4H)/Re$. The results for the parallel-plate channel are also given in the table and

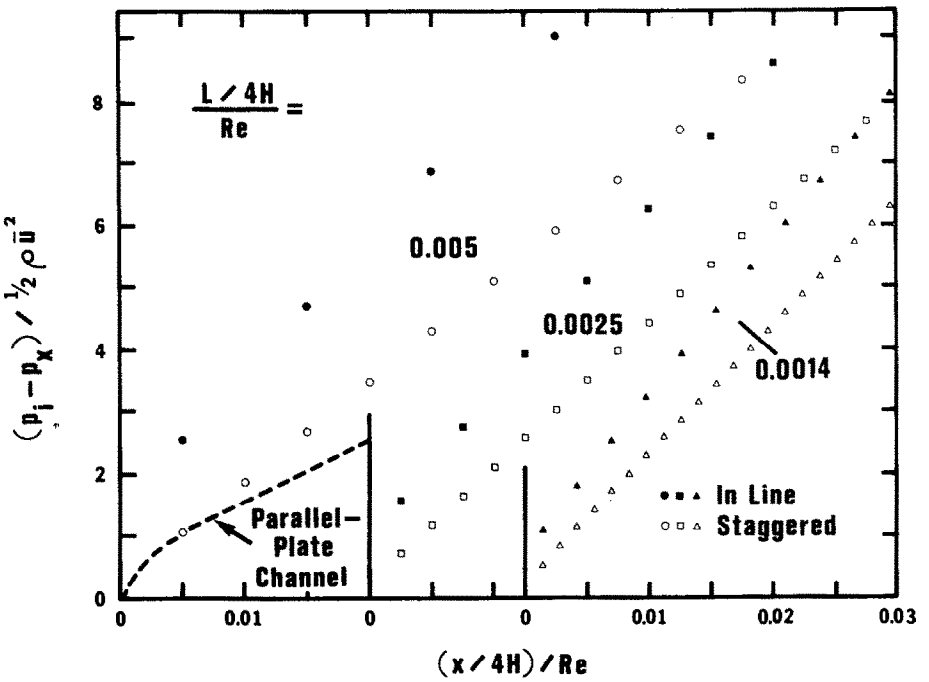

FIG. 4. Dimensionless pressure drop – range of larger $(L/4H)/Re$.

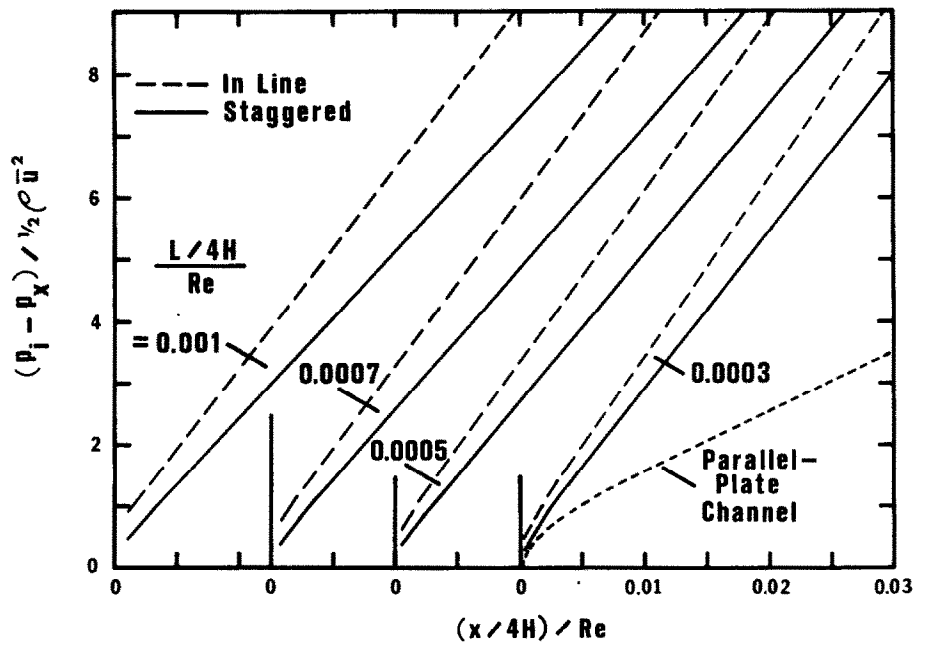

FIG. 5. Dimensionless pressure drop – range of smaller $(L/4H)/Re$.

Table 1. Results for the fully developed regime

	$\overline{Nu}_p$		fRe	
$(L/4H)/Re$	In-line	Stagg.	In-line	Stagg.
0.0003	24.6	23.5	288	256
0.0005	23.6	22.4	276	239
0.0007	22.8	21.5	268	228
0.0010	21.8	20.6	259	216
0.0014	20.9	19.5	250	204
0.0025	19.1	17.6	234	185
0.0050	17.0	14.9	217	162
∞	7.54	7.54	96	96

are identified by $(L/4H)/Re = \infty$. It can be seen from the table that the highest fully developed Nusselt numbers and friction factors occur in the presence of the shortest plates, that is, at the smaller values of $(L/4H)/Re$. With increasing plate length, both $\overline{Nu}_p$ and fRe decrease monotonically, but even for the largest value of $(L/4H)/Re$ considered here they are substantially larger than the corresponding parallel-plate results. The deviations between the two arrays are least for short plates ($4\frac{1}{2}$ and 12% for $\overline{Nu}_p$ and fRe for the first line of the table) but become substantially greater for longer plates (13 and 29% for the last line of the table).

PERFORMANCE COMPARISONS

As was discussed in the Introduction, the appraisal of the possible benefits of using augmented heat-transfer surfaces depends on the goal(s) to be fulfilled and the constraints being imposed. Here, successive consideration will be given to two basic constraints – constant mass flow rate and constant pumping power. Various goals will be identified during the course of the discussion.

Constant mass flow rate

In addition to the constant mass flow constraint, the performance comparisons will be made for segmented plate heat exchangers having the same frontal area and with the same value of the transverse plate spacing H (see Fig. 1). These same constraints will also be employed for comparisons with the parallel-plate channel, except that the spacing between the plates is $2H$. It may be noted that these conditions correspond to a constant Reynolds number. Furthermore, the constancy of the mass flow means that the magnitudes of the respective ε values provide a direct measure of the heat-transfer rates for the various heat exchangers.

The values of ε and of $\Delta p/\frac{1}{2}\rho\bar{u}^2$ will now be compared for in-line, staggered, and parallel-plate heat exchangers having the same heat-transfer surface area. It has already been pointed out that to achieve the same transfer area, the staggered array is one row longer than the in-line array. If L_{ex} denotes the streamwise length of the exchanger, then, for example, in-line plate arrays with $L_{ex} = 9L, 19L, \ldots$ have the same transfer surface area as staggered plate arrays with $L_{ex} = 10L, 20L, \ldots$. Furthermore, the length of the equal-area parallel-plate channel is $10L$, $20L \ldots$.

To establish the trends, it is sufficient to show the results for $L_{ex}/L = 9(10)$ and 19(20), respectively in the (a) and (b) parts of Table 2, where the notation 9(10) and 19(20) reflects the discussion of the preceding paragraph. The ε and $\Delta p/\frac{1}{2}\rho\bar{u}^2$ values listed in the table are taken from Figs. 2–5 and are parameterized by $(L/4H)/Re$ which, for the present conditions, is a direct reflection of the plate length.

The table shows that, as expected, both the effectiveness and the pressure drop increase as the surface area increases. However, of greater significance from the standpoint of optimal design is the fact that at small and intermediate values of ε, the effectivenesses

Table 2. Performance comparisons at constant mass flow and constant heat-transfer surface area

	ε			$\Delta p/\frac{1}{2}\rho\bar{u}^2$		
$(L/4H)/Re$	IL	Stagg.	P-P Ch.	IL	Stagg.	P-P Ch.
	(a) $L_{ex}/L = 9(10)$					
0.0003	0.400	0.382	0.221	1.32	1.13	0.766
0.0005	0.527	0.504	0.293	1.83	1.54	1.03
0.0007	0.623	0.597	0.354	2.32	1.92	1.26
0.0010	0.728	0.699	0.434	3.02	2.46	1.57
0.0014	0.819	0.791	0.525	3.92	3.16	1.96
0.0025	0.936	0.916	0.706	6.26	4.90	3.02
0.0050	0.992	0.984	0.901	11.2	8.36	5.38
	(b) $L_{ex}/L = 19(20)$					
0.0003	0.608	0.587	0.324	2.19	1.90	1.15
0.0005	0.760	0.737	0.438	3.33	2.73	1.57
0.0007	0.849	0.828	0.525	4.19	3.51	1.96
0.0010	0.922	0.906	0.642	5.61	4.62	2.54
0.0014	0.966	0.955	0.742	7.42	6.02	3.30
0.0025	0.996	0.993	0.901	12.1	9.53	5.39
0.0050	1.00	1.00	0.989	22.0	16.5	10.14

of the augmented arrays are resoundingly higher than those of the parallel-plate channel. These gains in effectiveness are sufficiently great so that the pressure drop penalty may be tolerable. Indeed, as will now be demonstrated, the higher heat transfer per unit exchanger length for the augmented arrays can lead to a lower pressure drop if the heat duty is fixed and the exchanger area is correspondingly adjusted.

Under the condition of constant mass flow, a fixed heat duty is equivalent to a fixed value of ε. Suppose that for $(L/4H)/Re = 0.0005$, the three configurations are compared at a constant heat duty given by $\varepsilon \sim 0.59$, the corresponding pressure drops $\Delta p/\frac{1}{2}\rho\bar{u}^2$ and exchanger lengths $(L_{ex}/4H)/Re$ are listed below.

	$\Delta p/\frac{1}{2}\rho\bar{u}^2$	$(L_{ex}/4H)/Re$
In-line	2.11	0.55
Staggered	1.90	0.65
Parallel-plate channel	2.28	1.73

This listing indicates that the pressure drop for the parallel-plate channel is the highest of all. Of even greater significance is that its length (and surface area) is $2\frac{1}{2}$–3 times greater than those of the augmented arrays. Therefore, the use of an augmented array results in a very substantial materials savings and a slight decrease in pressure drop.

The benefits of using an augmented array diminish (and become negative) at higher values of ε, as can be surmised from Table 2. It may also be noted in Table 2 that while there may be a possible balancing out of ε and Δp between the in-line and staggered arrays at low and intermediate ε, the balance tips in favor of the latter at higher ε. Since the greatest utility of the augmented arrays lies in the range of low and intermediate ε, both the in-line and staggered configurations should be evaluated before a final selection is made.

Constant pumping power

The comparisons at constant pumping power will be made under the condition of fixed heat-transfer surface area, and the objective is to determine which of the configurations yields the highest heat-transfer rate. For the in-line and staggered arrays, the same L and H are used, and the corresponding spacing for the parallel-plate channel is $2H$.

The pumping power P may be evaluated from its definition

$$P = (\dot{m}/\rho)\Delta p \tag{21}$$

which, after rearrangement, becomes

$$P = (\mu^3/128\rho^2H^2)(\Delta p/\tfrac{1}{2}\rho\bar{u}^2)Re^3. \tag{22}$$

Since the first factor on the RHS is a constant for the comparisons contemplated here, the constant pumping power constraint is equivalent to $(\Delta p/\frac{1}{2}\rho\bar{u}^2)Re^3 = \text{constant}$. From this, it follows that to fulfill the P = constant condition, the Reynolds numbers for the various configurations will be different, depending on the extent of the pressure-drop differences. The Reynolds numbers for the various configurations will also be reported here.

The computational procedure will now be described for determining the heat-transfer rates for the various configurations corresponding to constant pumping power and constant surface area. For this purpose, let IL and S respectively denote the in-line and staggered arrays, and let * denote the parallel-plate channel. The approach adopted is to compute $(Q_{IL}/Q^*)_P$ and $(Q_S/Q^*)_P$, thereby comparing each of the augmented arrays with the parallel-plate channel. Furthermore, by comparing the values of the two ratios and noting that the same value of Q_P^* is common to both, the heat-transfer capabilities of the two arrays may be identified.

Consider, for concreteness, the determination of $(Q_S/Q^*)_P$ for a staggered-array heat exchanger geometry defined by given values of L/H, L_{ex}/L, and $L_{ex}/H = (L_{ex}/L)(L/H)$. First, a Reynolds number Re_S is selected, and the quantities $(L/4H)/Re$ and $(L_{ex}/4H)/Re$ are evaluated. With these, ε_S and $(\Delta p/\frac{1}{2}\rho\bar{u}^2)_S$ can be read from Figs. 2–5, and $(Re^3(\Delta p/\frac{1}{2}\rho\bar{u}^2))_S$ is then determined. Next, for a parallel-plate channel having an L_{ex}/H equal to that of the staggered array, a graph of $(Re^3(\Delta p/\frac{1}{2}\rho\bar{u}^2))^*$ vs Re^* is generated using the information of Figs. 4 or 5 (or the corresponding computer listing). From this graph, the value of Re^* can be identified for which the pumping power for the staggered array and the parallel-plate channel are equal. With this Reynolds number, $((L_{ex}/4H)/Re)^*$ can be computed and ε^* read from Figs. 2 or 3.

The heat-transfer rates for the two cases can be written as

$$Q_S = (\dot{m}c_p(T_{bx} - T_i))_S,$$

$$Q^* = (\dot{m}c_p(T_{bx} - T_i))^* \tag{23}$$

so that

$$(Q_S/Q^*)_P = (\varepsilon Re)_S/(\varepsilon Re)^* \tag{24}$$

where the subscript P is appended to denote constant pumping power.

The ratio $(Q_{IL}/Q^*)_P$ is determined by following steps identical to those outlined for the determination of $(Q_S/Q^*)_P$, but with special care taken to ensure equality of the heat-transfer surface areas. Thus, for example, a value of $L_{ex}/L = 9$ for an in-line array corresponds to the same surface area as does $L_{ex}/L = 10$ for the parallel-plate channel and the staggered array.

The $(Q/Q^*)_P$ ratios for the in-line and staggered arrays are presented in Figs. 6 and 7. These figures correspond respectively to $L/H = 2$ and 5, where these values were chosen to reflect current practice. In each figure, results are given for heat exchanger lengths L_{ex}/L ranging from 9(10) to 99(100) – these dimensionless lengths being indicative of the number of rows in the heat exchanger. The abscissa is the Reynolds

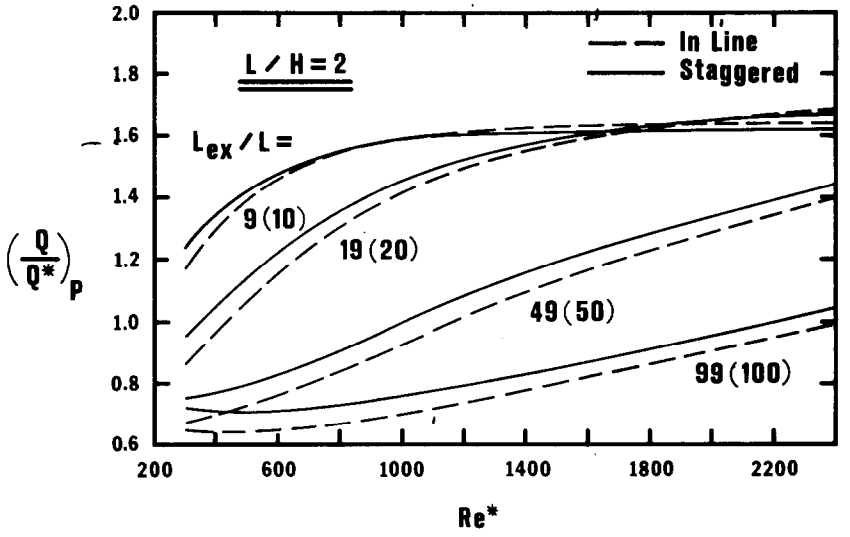

FIG. 6. Heat-transfer performance for constant pumping power and constant transfer surface area, $L/H = 2$.

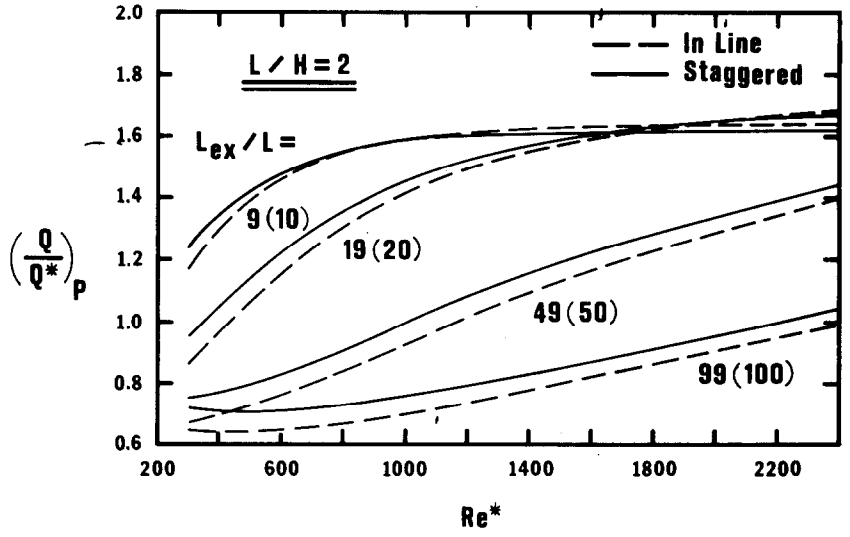

FIG. 7. Heat-transfer performance for constant pumping power and constant transfer surface area, $L/H = 5$.

number Re^* for the parallel-plate channel, the values of which span the practical range where laminar flow might be expected to exist.

In appraising the results, special attention is given to the ordinate value $(Q/Q^*)_P = 1$. This represents the boundary between conditions where the use of segmented plates either does or does not increase the heat-transfer rate relative to the parallel-plate channel. Inspection of the figures shows that there is a wide range of geometrical and operating conditions where the use of segmented plates is beneficial. In general, positive benefits are realized for shorter heat exchangers and at higher Reynolds numbers. For favorable conditions, values of $(Q/Q^*)_P \sim 1.6$ can be attained.

Both shorter heat exchangers and higher Reynolds numbers tend to bring about lower values of the effectiveness ε. With this realization, a careful study was made to identify the range of effectiveness values where $(Q/Q^*)_P > 1$. It was found that if $\varepsilon^* < 0.70$–0.75, $(Q_S/Q^*)_P > 1$ and that if $\varepsilon^* < 0.65$–0.70, then $(Q_{IL}/Q^*)_P > 1$. Therefore, with these criteria, an indication can readily be obtained of whether or not there are positive benefits of using segmented plates. These criteria are particularly convenient because they are based on the readily available effectiveness values for the parallel-plate channel.

Further examination of Figs. 6 and 7 indicates that the heat-transfer rates provided by the staggered array are generally higher than those for the in-line array. Thus, on the basis of heat-transfer considerations alone, there is ample justification to select the stag-

gered array in preference to the in-line array.

The Reynolds number relationships necessary to fulfill the constant pumping power – constant surface area constraints are shown in Figs. 8 and 9, respectively for $L/H = 2$ and 5. In these figures, the Re_S and Re_{IL} which fulfill these constraints are plotted as a function of Re^*, with L_{ex}/L as curve parameter. For orientation purposes, a line $Re = Re^*$ is also plotted on each figure.

It is seen from these figures that the Reynolds numbers for the segmented-plate arrays are smaller than those for the parallel-plate channel. Furthermore, among the two arrays, the Reynolds numbers for the in-line plates are lower than those for the staggered plates. If the heat exchanger were located in a flow circuit where there are other significant sources of pressure drop, then the reduction in Reynolds number (i.e. in mass flow) might have important fringe benefits

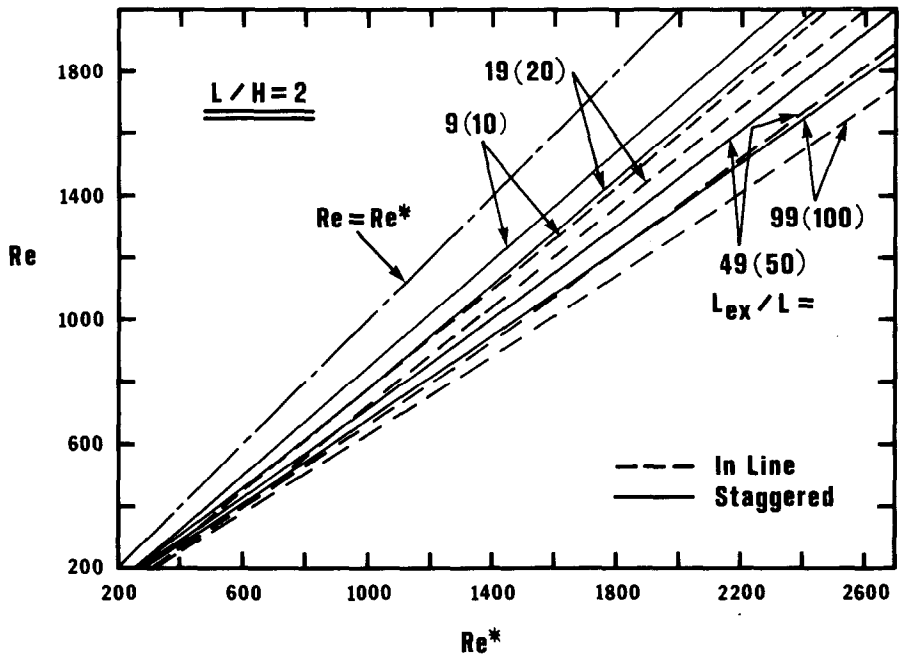

FIG. 8. Reynolds number relationships for constant pumping power and constant heat-transfer surface area, $L/H = 2$.

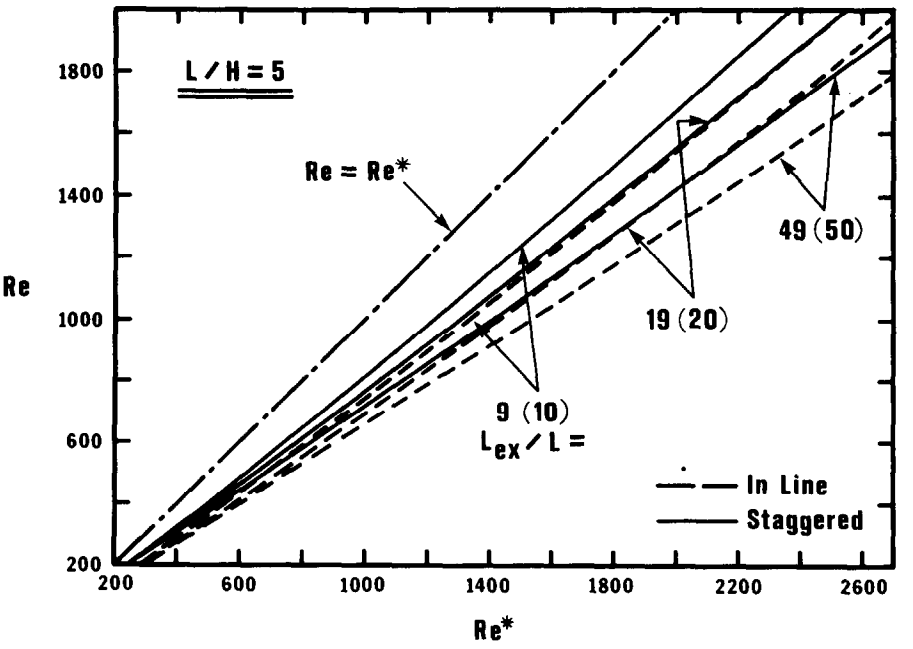

FIG. 9. Reynolds number relationships for constant pumping power and constant heat-transfer surface area, $L/H = 5$.

in lowering the overall system pressure drop. In particular, the in-line array provides the opportunity for greater benefits of this type. Because of this, there may be advantages in adopting this array even though it may offer less heat-transfer enhancement than the staggered array.

CONCLUDING REMARKS

The present analysis has provided basic heat-transfer and pressure-drop information for in-line and staggered segmented-plate arrays and has employed this information in performance comparisons. The basic quantities presented are the effectiveness ε and the dimensionless pressure drop $\Delta p/\frac{1}{2}\rho\bar{u}^2$, and these depend on a single parameter, $(L/4H)/Re$. Results are given both for the development and fully developed regimes.

For a fixed mass flow rate and fixed heat-transfer surface area, the effectivenesses of the segmented-plate arrays are substantially higher than that of the parallel-plate channel, both in the range of small and intermediate effectiveness values. Correspondingly, the segmented arrays give rise to higher pressure drops. It was demonstrated that the higher heat transfer per unit exchanger length of the segmented arrays can prove highly advantageous in the case of a fixed heat duty. In an example at constant mass flow, it was shown that a given heat duty can be handled by a segmented array at a lower pressure drop and with only a third of the surface area, compared with the parallel-plate channel.

Performance curves corresponding to constant pumping power and constant surface area were developed for the two segmented arrays and for the parallel-plate channel. Relative to the parallel-plate channel, the segmented arrays provide higher heat-transfer rates when the effectiveness ε^* of the channel is less than 0.65–0.75. This criterion facilitates a first-round decision about whether or not it is beneficial to use a segmented-plate array compared with a parallel-plate channel.

Comparisons were also made between the in-line and staggered arrays. At a fixed mass flow and fixed surface area, the former yields a slightly higher effectiveness, but with a pressure-drop increment (i.e. increase) that is larger than the increment in effectiveness. For constant pumping power and constant surface area, the heat transfer provided by the staggered array exceeds that of the in-line array, but at the price of a higher mass flow (which may result in higher pressure drops in other system components). If the heat exchanger alone were to be taken into account, then the staggered array appears superior. On the other hand, if the pressure drop in other system components exceeds that of the heat exchanger, then the in-line array may be as attractive (or, perhaps, even more attractive) as the staggered array.

Acknowledgement – This research was supported, in part, by ONR Contract N00014-76-C-0246.

REFERENCES

1. R. H. Norris and W. A. Spofford, High performance fins for heat transfer, *Trans. Am. Soc. Mech. Engrs* **64**, 489–496 (1942).
2. W. H. Kays and A. L. London, *Compact Heat Exchangers*, 2nd edn. McGraw-Hill, New York (1964).
3. R. K. Shah and A. L. London, Offset rectangular plate-fin surfaces—heat transfer and flow friction characteristics, ASME *J. Engng Pwr* **90**, 218–228 (1968).
4. A. R. Wieting, Empirical correlation for heat transfer and flow friction characteristics of rectangular offset-fin plate-fin heat exchangers, *J. Heat Transfer* **97C**, 488–490 (1975).
5. S. Mochizuki and Y. Yoshinao, Heat transfer and friction characteristics of strip fins, *Heat Transfer, Japanese Res.* **6**(3), 36–59 (1977).
6. E. M. Sparrow, B. R. Baliga and S. V. Patankar, Heat transfer and fluid flow analysis of interrupted-wall channels, with application to heat exchangers, *J. Heat Transfer* **99**, 4–11 (1977).
7. A. E. Bergles, Survey and evaluation of techniques to augment convective heat and mass transfer, in *Progress in Heat and Mass Transfer*, Vol. 1, pp. 331–424. Pergamon Press, Oxford (1969).
8. A. E. Bergles, R. R. Blumenkrantz and J. Taborek, Performance evaluation criteria for enhanced heat transfer surfaces, in *Proceedings, Fifth International Heat Transfer Conference*, Vol. 2, Paper FC6.3, pp. 239–243 (1974).
9. A. E. Bergles, G. H. Junkhan and R. L. Bunn, Performance criteria for cooling systems on agricultural and industrial machines, Report HTL-6, Department of Mechanical Engineering, Iowa State University, Ames, Iowa (December 1974).
10. S. V. Patankar and D. B. Spalding, *Heat and Mass Transfer in Boundary Layers*, 2nd edn. Intertext, London (1970).
11. W. E. Mercer, W. M. Pearce and J. E. Hitchcock, Laminar forced convection in the entrance region between parallel plates, *J. Heat Transfer* **89C**, 251–257 (1967).

FORMULES CONCERNANT LE TRANSFERT THERMIQUE, LA PERTE DE CHARGE ET LES PERFORMANCES POUR DES ECHANGEURS DE CHALEUR A PLAQUES EN LIGNE ET EN QUINCONCE

Résumé—A partir des solutions numériques des équations du mouvement et de l'énergie, on étude les résultats de transfert thermique et de perte de charge pour un écoulement laminaire d'air entre des rangées de segments de plaque, en ligne ou en quinconce. Les résultats dépendent d'un unique paramètre sans dimension qui concerne la géométrie et les paramètres de l'écoulement. Une application des résultats est faite pour comparer la performance de deux types de rangées de plaques entre eux et avec le cas du canal entre plaques parallèles. A débit massique constant et à surface de plaque constante, l'efficacité ε de transfert thermique des rangées de plaques est nettement plus élevée que pour le canal continu, dans le domaine des efficacités faibles aussi bien qu'intermédiaire. De plus, pour un flux fixé, correspondant à une valeur intermédiaire de ε, et pour un débit massique constant, la surface d'échange des rangées segmentées est seulement un tiers environ de celle du canal à plaques parallèles. Pour une puissance de pompage constante et une surface d'échange constante, le flux thermique pour les rangées segmentées dépasse celui du canal à plaques parallèles lorsque l'efficacité de celui-ci est inférieure à 0,65–0,75. Dans de nombreuses conditions, l'arrangement en quinconce donne de meilleures performances que l'arrangement en ligne, mais on identifie des situations où on a le contraire.

BEZIEHUNGEN FÜR WÄRMEÜBERGANG, DRUCKVERLUST UND LEISTUNG VON FLUCHTENDEN, VERSETZTEN UND DURCHGEHENDEN PLATTENWÄRMETAUSCHERN

Zusammenfassung—Durch numerische Lösung der Bewegungs- und Energiegleichungen wurden grundlegende Ergebnisse für Wärmeübergang und Druckverlust bei laminarer Luftströmung durch fluchtende oder versetzte Anordnungen von Plattensegmenten gewonnen. Die Ergebnisse hängen nur von einem dimensionslosen Parameter ab, der die wesentlichen Größen der Geometrie und der Strömung umfaßt. Die Ergebnisse wurden dazu verwendet, die Leistung von 2 Typen geteilter Plattenanordnungen miteinander und mit einem Kanal aus parallelen Platten zu vergleichen. Bei gleichem Massenstrom und gleicher wärmeübertragender Oberfläche ist der Wirkungsgrad ε der Wärmeübertragung bei den geteilten Anordnungen merklich größer als bei dem Kanal mit parallelen Platten, sowohl bei Wirkungsgraden im unteren als auch im mittleren Bereich. Darüber hinaus beträgt bei gegebener Wärmeleistung, entsprechend einem mittleren ε-Wert, und bei gleichem Massenstrom die Wärmeübertragungsfläche der geteilten Anordnungen nur etwa ein Drittel derjenigen des Kanals mit parallelen Platten. Bei gleicher Gebläseleistung und gleichen Oberflächenbedingungen ist der Wärmeübergang bei den geteilten Anordnungen höher als bei dem Kanal mit parallelen Platten, wenn der Wirkungsgrad bei letzterem kleiner als 0,65–0,75 ist. Unter den meisten Bedingungen erbringt die versetzte Anordnung eine bessere Leistung als die fluchtende, aber es gibt auch Situationen, bei denen es umgekehrt ist.

СООТНОШЕНИЯ МЕЖДУ ИНТЕНСИВНОСТЬЮ ТЕПЛООБМЕНА, ПЕРЕПАДОМ ДАВЛЕНИЯ И ГЕОМЕТРИЧЕСКИМИ ХАРАКТЕРИСТИКАМИ ТЕПЛООБМЕННИКОВ С КОРИДОРНЫМ И ШАХМАТНЫМ РАСПОЛОЖЕНИЕМ РЕБЕР И С ГЛАДКИМ ПЛОСКОПАРАЛЛЕЛЬНЫМ КАНАЛОМ

Аннотация — С помощью численного решения уравнений движения и энергии получены результаты по теплообмену и перепаду давления при ламинарном течении воздуха через каналы, составленные из отрезков пластин, расположенных в коридорном и шахматном порядке. Результаты зависят от единственного безразмерного параметра, включающего соответствующие геометрические размеры и характеристики потока. На основе этих результатов было проведено сравнение режимов работы теплообменников, составленных из гладких плоскопараллельных каналов и каналов с коридорным и шахматным расположением ребер. При постоянном массовом расходе и постоянной площади поверхности теплообмена эффективность теплообмена ε у поверхностей оребренных пластин намного выше, чем у плоскопараллельного канала как в области малых, так и промежуточных значений эффективности. Кроме того, при фиксированной тепловой нагрузке, соответствующей промежуточному значению ε, и при постоянном массовом расходе оребренная поверхность теплообмена составляет примерно треть поверхности теплообмена плоскопараллельного канала. При постоянной мощности, затрачиваемой на прокачку теплоносителя, и постоянных условиях на поверхности интенсивность теплообмена при наличии оребрения выше, чем в плоскопараллельном канале, когда эффективность последнего ниже 0,65–0,75. В большинстве случаев рабочие характеристики теплообменников с шахматным расположением ребер лучше, чем у теплообменников с коридорным расположением, но возможны и обратные ситуации.